frontiers | Frontiers in Physics

ORIGINAL RESEARCH
published: 09 May 2022
doi: 10.3389/fphy.2022.907718

Synthesis Design of Dual-Band Filtering Power Dividers Based on E-Shape Resonators

Jiwei Shen[1], Wei Li[2], Kang Ping[2], Zhuowei Zhang[2] and Minghan Shu[2]*

[1]ZiJin College Nanjing University of Science and Technology, Nanjing, China, [2]Nanjing Normal University, Nanjing, China

In this study, a comprehensive design of dual-band filtering power dividers (FPDs) with arbitrary phase distribution is presented. With a series of analytical equations for the direct synthesis design, the proposed method shows its great capacity of designing dual-band FPDs with any pre-specified responses, arbitrary phase distribution, and high isolation. To verify this design method, a demonstrated dual-band FPD with 90° phase differences between two outputs based on E-shape resonators has been implemented. The emulational results coincide with the measured results well, showing the feasibility of the proposed method.

Keywords: direct synthesis design, filtering power divider, dual-band, phase distribution, isolation

OPEN ACCESS

Edited by:
Kai-Da Xu,
Xi'an Jiaotong University, China

Reviewed by:
Baoping Ren,
East China Jiaotong University, China
Zhi-Chong Zhang,
Jinggangshan University, China

****Correspondence:***
Zhuowei Zhang
zhuowei_zhang@163.com

Specialty section:
This article was submitted to Optics and Photonics, a section of the journal Frontiers in Physics

Received: *30 March 2022*
Accepted: *11 April 2022*
Published: *09 May 2022*

Citation:
Shen J, Li W, Ping K, Zhang Z and Shu M (2022) Synthesis Design of Dual-Band Filtering Power Dividers Based on E-Shape Resonators. Front. Phys. 10:907718. doi: 10.3389/fphy.2022.907718

INTRODUCTION

A bandpass filter (BPF) and power divider (PD) are the indispensable components in various modern wireless communication systems. In general, they often integrate into a single component for miniaturization and improved performance, i.e., filtering power divider (FPD) [1–6], which provides both function of power division and filtering simultaneously. In the meantime, future mobile communication can provide mobile terminal online HD video virtual reality (VR), augmented reality (AR), and such wireless interactive services that require big data traffic and high transmission quality [7, 8]. The phase shifter is the critical component for the multi-polarization and multi-beam technology, which plays an important role in the construction of mobile communication systems with high-speed data transmission and efficient spectrum utilization.

In recent years, there are few research studies on filtering power dividers with an arbitrary phase difference [9–11]. For instance, in [9], a new class of filtering power divider that integrates the filter's PD, phase shifter, and impedance transformer into a single component was proposed, which achieves a good result in filtering power division response and phase difference. Moreover, in [10], a filtering power divider consisting of a Wilkinson power divider (WPD) and N_{th}-order-coupled line bandpass filters was proposed, and closed-form design equations are derived.

Unfortunately, they are only single-band filtering power divider with a phase difference; as the author knows, there are few dual-band filtering power dividers with a phase difference.

In this study, a new synthesis design method of dual-band FPD with arbitrary phase distribution is proposed. Based on a series of analytical equations and synthesis design, a dual-band FPD with any prescribed specifications including filtering power division response, isolation, and phase shifter can be obtained. To verify the proposed design concept, a dual-band FPD with 90° port-to-port phase distribution based on E-shape resonators has been designed and fabricated.

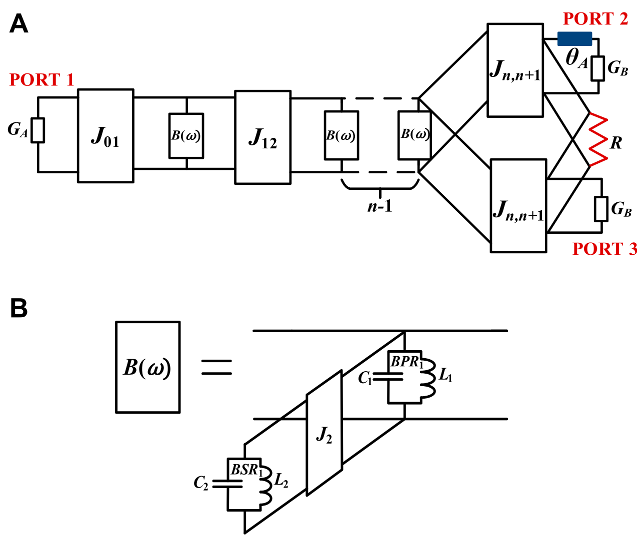

FIGURE 1 | (A) Topology of *n*th-order dual-band FPD. **(B)** Inverter-coupled resonator sections $B(\omega)$.

DESIGN AND ANALYSIS

Figure 1A describes a new general nth-order dual-band FPD topology, which is mainly made up of multiple dual-frequency resonant units B (ω), one branch line θ_A, and one isolation resistor R. Specifically, for dual-number operation bands, every dual-frequency resonant unit consists of one bandpass resonator (BPR_1) and one inverter-coupled bandstop resonators (BSR_1) as shown in **Figure 1B**. The signal comes from port #1, flowing through multiple dual-frequency resonant units, and finally outputs from port #2 and port #3. Due to the branch line and isolation resistor, the two outputs can achieve phase difference and isolation at the same time.

Analysis of Filtering Power Division Response

On the bias of the frequency transformation and prototype synthesis technique, the prescribed dual-band filtering power division response can be obtained step by step. In the first step, the admittance of inverter-coupled resonators in **Figure 1B** viewed from the input/output is derived by:

$$B(\omega) = jT(\omega) = jb_1\left(\frac{\omega}{\omega_{01}} - \frac{\omega_{01}}{\omega}\right) + \frac{J_2}{jb_2\left(\frac{\omega}{\omega_{02}} - \frac{\omega_{02}}{\omega}\right)},$$
$$b_i = \omega_{0i}C_{0i}, \omega_{0i} = 1\Big/\sqrt{C_{0i}L_{0i}}, i = 1, 2, 3...m., \tag{1}$$

where ω_{0i} and b_i represent the angular resonant frequency and susceptance slope parameter of the ith resonator, respectively.

Assuming that the FPD has two passbands of (ω_{L1}, ω_{H1}) and (ω_{L2}, ω_{H2}), the lower limits of the two passbands (ω_{L1}, ω_{L2}) ought to map to −1 in the normalized domain, while the upper limits (ω_{H1}, ω_{H2}) ought to map to +1 in the normalized domain. The parameters that define the transformation (ω_{01}, ω_{02}, b_1, and b_2) can finally be expressed as the functions of the two passband limits (ω_{L1}, ω_{H1}, and ω_{L2}, ω_{H2}) according to the relationship between the roots and the coefficients of the equation of $T(\omega) = 1$. Since the function $U(\omega) = T(\omega)$-1 denotes the ratio of two polynomials, we can further use $Q(\omega)$ to represent the numerator of $U(\omega)$ as:

$$Q(\omega) = \omega^4 + d_3\omega^2 + d_2\omega^2 + d_1\omega + d_0. \tag{2}$$

Once the aforementioned frequencies are prescribed according to specifications in advance, the parameters ($\omega_{01,}$ ω_{02}) and ($b_{1,}$ b_2) can be calculated as:

$$\begin{aligned}\omega_{01} &= \sqrt{-\frac{d_0 d_3}{d_1}},\\ \omega_{02} &= \sqrt{-\frac{d_1}{d_3}},\\ b_1 &= \sqrt{-\frac{d_0}{d_1 d_3}},\\ b_2 &= \sqrt{-\frac{d_1}{d_3}}\,\frac{d_1 d_3^2}{d_1 d_2 d_3 - d_1^2 - d_0 d_3^2}.\end{aligned} \tag{3}$$

Afterward, by mapping the nth-order dual-band FPD topology to its corresponding low-pass prototype, the inverters' values can be finally expressed as [12]:

$$J_{01} = \sqrt{\frac{G_A}{g_0 g_1}},\quad J_{\mathrm{i,i+1}} = \sqrt{\frac{1}{g_{\mathrm{i}} g_{\mathrm{i+1}}}},\quad J_{n,n+1} = \sqrt{\frac{G_B}{2g_n g_{n+1}}}. \tag{4}$$

Afterward, the coupling coefficients between the adjacent BPRs can be derived as:

$$k_{i,i+1} = \frac{J_{i,i+1}}{b_1}. \tag{5}$$

Meanwhile, the coupling coefficient between the BSR and BPR can be derived as:

$$k_i = \frac{J_i}{\sqrt{b_1 b_i}}. \tag{6}$$

In addition, the external quality factors can be formulated by:

$$Q_{in} = \frac{b_1 G_A}{J_{01}^2},\ Q_{out} = \frac{b_1 G_B}{J_{n,n+1}^2}. \tag{7}$$

After the dual-band filtering power division responses are analyzed, the isolation and phase distribution can be obtained by

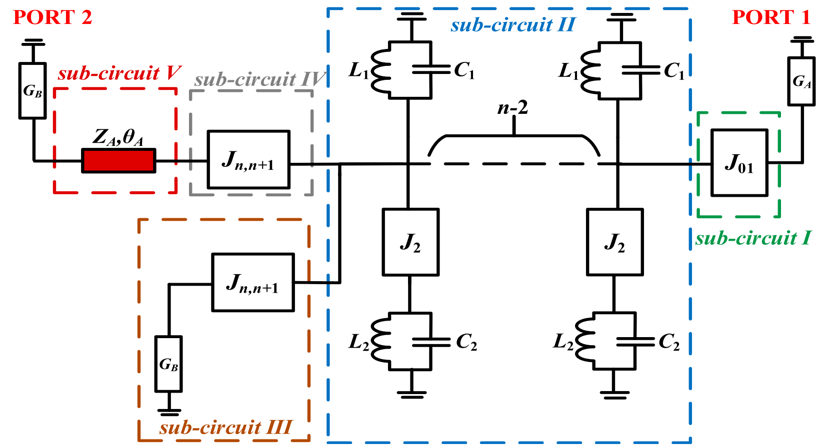

FIGURE 2 | Equivalent circuit diagram for analyzing phase difference between two output ports.

means of the isolation resistor R and the branch lines, respectively.

Analysis of Phase Difference Between Outputs

In order to analyze the phase difference between the output ports of the dual-band filtering power division network topology, the ABCD matrix of the whole circuit is solved through the microwave network analysis method. Furthermore, the insertion phase shifts $\angle S_{12}$ and $\angle S_{13}$ can be deduced.

First, $\angle S_{12}$ is analyzed. Assuming that the incident wave is only introduced in port #1 and output in port #2 ($G_A = G_B = Y_0$), the topology diagram of the dual-band filtering power division network with phase-shifting function in **Figure 1A** is appropriately simplified and redrawn, as shown in **Figure 2**. There are five sub-circuits in this schematic, as denoted by sub-circuit I, sub-circuit II, sub-circuit III, sub-circuit IV, and sub-circuit V.

For dual-frequency resonant units $B(\omega)$, its input admittance P can be represented as:

$$P = P_1 + \frac{J_2^2}{P_2}, \tag{8}$$

where $P_1 = j\omega C_1$ is represented as the square root of capacitances of BPR and BSR in the low-pass prototype, where the value of eac+$1/j\omega L_1$, $P_2 = j\omega C_2+1/j\omega L_2$, and P_1 and P_2 are the admittances of the corresponding resonators. For sub-circuit I, its ABCD matrix can be obtained as:

$$\begin{pmatrix} A_1 & B_1 \\ C_1 & D_1 \end{pmatrix} = \begin{pmatrix} 0 & \frac{1}{jJ_{01}} \\ -jJ_{01} & 0 \end{pmatrix}. \tag{9}$$

For sub-circuit II, its ABCD matrix can be obtained as:

$$\begin{pmatrix} A_2 & B_2 \\ C_2 & D_2 \end{pmatrix} = \begin{pmatrix} 1 & 0 \\ N_1 & 1 \end{pmatrix}, \tag{10}$$

where

$$N_1 = P + \cfrac{J_{n-1,n}^2}{P + \cfrac{J_{n-2,n-1}^2}{P + \dots}}.$$
$$\ddots$$
$$P + \frac{J_{12}^2}{P}$$

Meanwhile, for sub-circuits III, IV, and V, their ABCD matrix can be obtained, respectively, as follows:

$$\begin{pmatrix} A_3 & B_3 \\ C_3 & D_3 \end{pmatrix} = \begin{pmatrix} 1 & 0 \\ \frac{J_{n,n+1}^2}{Y_0} & 1 \end{pmatrix}, \tag{11}$$

$$\begin{pmatrix} A_4 & B_4 \\ C_4 & D_4 \end{pmatrix} = \begin{pmatrix} 0 & \frac{1}{jJ_{n,n+1}} \\ -jJ_{n,n+1} & 0 \end{pmatrix}, \tag{12}$$

$$\begin{pmatrix} A_5 & B_5 \\ C_5 & D_5 \end{pmatrix} = \begin{pmatrix} \cos\theta_A & jZ_A \sin\theta_A \\ \frac{j\sin\theta_A}{Z_A} & \cos\theta_A \end{pmatrix}. \tag{13}$$

Finally, the ABCD matrix of the whole circuit can be solved as follows:

$$\begin{pmatrix} A_6 & B_6 \\ C_6 & D_6 \end{pmatrix}, \tag{14}$$

where

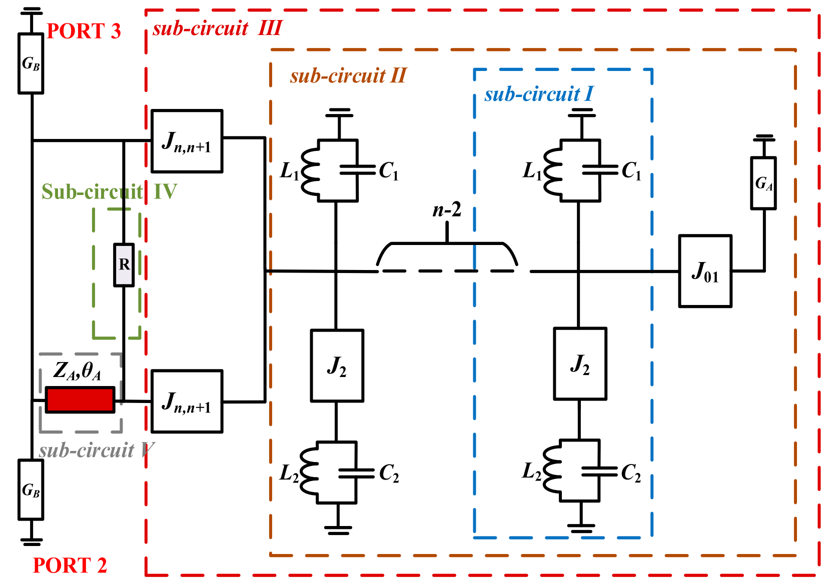

FIGURE 3 | Equivalent circuit diagram for analyzing isolation between two output ports.

$$A_6 = -\frac{J_{n,n+1}\cos\theta_A}{J_{01}} - \frac{j\left(J_{n,n+1}^2/Y_0 + N_1\right)\sin\theta_A}{J_{01}J_{n,n+1}Z_A},$$
$$B_6 = -\frac{\left(J_{n,n+1}^2/Y_0 + N_1\right)\cos\theta_A}{J_{01}J_{n,n+1}} - \frac{jJ_{n,n+1}Z_A\sin\theta_A}{J_{01}},$$
$$C_6 = -\frac{jJ_{01}\sin\theta_A}{J_{n,n+1}Z_A},$$
$$D_6 = -\frac{J_{01}\cos\theta_A}{J_{n,n+1}}.$$

Then, the insertion phase $\angle S_{12}$ can be obtained as:

$$\angle S_{12} = -\tan^{-1}\frac{B_6Y_0 + C_6/Y_0}{j(A_6+D_6)}. \qquad (15)$$

In a similar way, the insertion phase $\angle S_{13}$ can be obtained as:

$$\angle S_{13} = -\tan^{-1}\frac{B_7Y_0 + C_7/Y_0}{j(A_7+D_7)}, \qquad (16)$$

where

$$A_7 = -\frac{J_{n,n+1}}{J_{01}},$$
$$B_7 = -\frac{N_1 + J_{n,n+1}^2\left(1/Y_0 + jZ_A\cos\theta_A\right)}{J_{01}J_{n,n+1}},$$
$$C_7 = \theta_A,$$
$$D_7 = -\frac{J_{01}}{J_{n,n+1}}.$$

Once the phase shifts $\angle S_{12}$ and $\angle S_{13}$ are achieved, the phase difference between the output ports can be finally solved by subtracting the two equations ($\angle S_{12}$ and $\angle S_{13}$). Furthermore, the desired electrical length of the branch line can be obtained.

Analysis of Isolation Between Outputs

After analyzing the phase difference between outputs, the isolation can also be derived by means of the microwave network analysis method [13]. First, assuming that the incident wave is only introduced in port #2 and output in port #3 ($G_A = G_B = Y_0$), the topology diagram of the dual-band filtering power division network with phase-shifting function in **Figure 1A** is appropriately simplified and redrawn, as shown in **Figure 3**.

The equivalent circuit diagram has five sub-circuits, which are represented as sub-circuits I, II, III, IV, and V, respectively. As mentioned earlier, with the calculated admittance N_1 of sub-circuit II, the ABCD matrix of sub-circuit III can be deduced as:

$$\begin{pmatrix} A_1 & B_1 \\ C_1 & D_1 \end{pmatrix} = \begin{pmatrix} -1 & -\frac{N}{J_{n,n+1}^2} \\ 0 & -1 \end{pmatrix}. \qquad (17)$$

Then, we can attain the admittance matrix Y_1 of sub-circuit III with the following equation by conveniently transforming the ABCD matrix to its corresponding admittance matrix:

$$\mathbf{Y}_1 = \begin{pmatrix} \frac{D_1}{B_1} & \frac{B_1C_1 - A_1D_1}{B_1} \\ -\frac{1}{B_1} & \frac{A_1}{B_1} \end{pmatrix} = \begin{pmatrix} \frac{J_{n,n+1}^2}{N} & \frac{J_{n,n+1}^2}{N} \\ \frac{J_{n,n+1}^2}{N} & \frac{J_{n,n+1}^2}{N} \end{pmatrix}. \qquad (18)$$

In a similar way, the admittance matrix Y_2 of sub-circuit IV can be derived as:

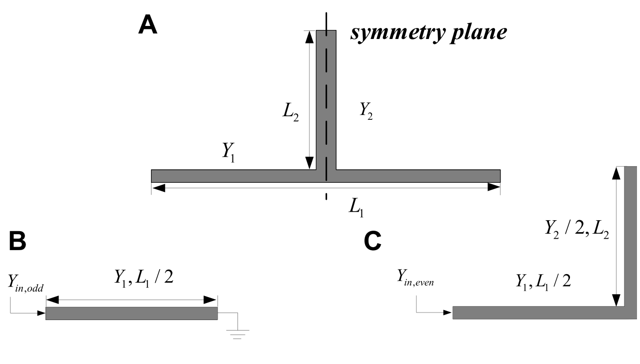

FIGURE 4 | (A) Structure of the employed E-shape resonator. **(B)** Odd-mode equivalent circuit. **(C)** Even-mode equivalent circuit.

$$\mathbf{Y}_2 = \begin{pmatrix} \frac{1}{R} & -\frac{1}{R} \\ -\frac{1}{R} & \frac{1}{R} \end{pmatrix}. \tag{19}$$

In the meantime, the ABCD matrix of sub-circuit V is shown as follows:

$$\begin{pmatrix} A_5 & B_5 \\ C_5 & D_5 \end{pmatrix} = \begin{pmatrix} \cos\theta_A & jZ_A \sin\theta_A \\ \frac{j\sin\theta_A}{Z_A} & \cos\theta_A \end{pmatrix}. \tag{20}$$

Then, the result of $Y_1 + Y_2$ should be converted into an ABCD matrix and cascaded with the ABCD matrix of sub-circuit V to find the whole ABCD matrix of the schematic that has been analytically derived as follows:

$$\begin{pmatrix} A_6 & B_6 \\ C_6 & D_6 \end{pmatrix}, \tag{21}$$

where

$$A_6 = \frac{N_3 R\left(N_3 + J_{n,n+1}^2 R\right)\cos\theta_A - 4jJ_{n,n+1}^2\left(N_3 - J_{n,n+1}^2 R\right)Z_A \sin\theta_A}{N_3 R\left(N_3 - J_{n,n+1}^2 R\right)},$$

$$B_6 = \frac{N_3 R\cos\theta_A + j\left(N_3 + J_{n,n+1}^2 R\right)Z_A \sin\theta_A}{N_3 - J_{n,n+1}^2 R},$$

$$C_6 = \frac{-4J_{n,n+1}^2\left(N_3 - J_{n,n+1}^2 R\right)Z_A\cos\theta_A + jN_3 R\left(N_3 + J_{n,n+1}^2 R\right)\sin\theta_A}{N_3 R\left(N_3 - J_{n,n+1}^2 R\right)Z_A},$$

$$D_6 = \frac{\left(N_3 + J_{n,n+1}^2 R\right)Z_A\cos\theta_A + jN_3 R\sin\theta_A}{\left(N_3 - J_{n,n+1}^2 R\right)Z_A}.$$

Till now, the scattering parameter S_{23} can be derived according to the conversion relationship between S parameter and transfer matrix, and then the isolation resistance R can be further obtained by setting $S_{23} = 0$. The solution formula of resistance R can be derived as follows:

$$R = \frac{H_1 + H_2}{H_3}, \tag{22}$$

where

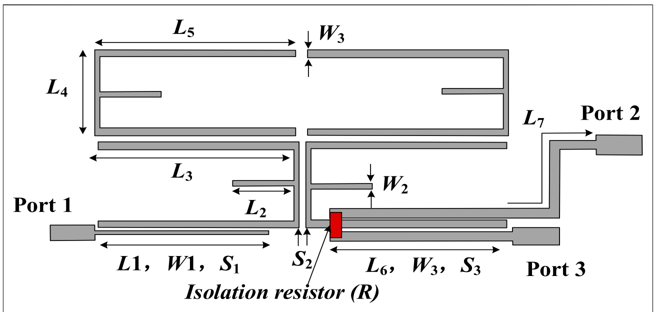

FIGURE 5 | Configuration of the proposed dual-band FPD with physical dimensions: $L_1 = 16.5$, $L_2 = 8.5$, $L_3 = 17$, $L_4 = 7.65$, $L_5 = 17.9$, $L_6 = 16.3$, and $L_7 = 24$, $W_1 = 0.36$, $W_2 = 0.3$, and $W_3 = 1.1$, $S_1 = 0.1$, $S_2 = 0.3$, and $S_3 = 0.1$ (all units: mm), and R = 195Ω. The design targets of the proposed dual-band FPD are given as follows: 1) Passbands 1: 1.87–1.92 GHz; 2) Passbands 2: 2.06–2.11 GHz; 3) Return loss: 20 dB; 4) Isolation: >20 dB; 5) Phase distribution: 90°.

$$\begin{aligned} H_1 &= -2\sqrt{J_{n,n+1}^8 - 2J_{n,n+1}^6 N_3} + 2J_{n,n+1}^4\cos^2\theta_A, \\ H_2 &= -J_{n,n+1}^2 N_3\cos^2\theta_A + 2J_{n,n+1}^4\sin^2\theta_A - J_{n,n+1}^2 N_3\sin^2\theta_A, \\ H_3 &= J_{n,n+1}^4\cos^2\theta_A + J_{n,n+1}^4\sin^2\theta_A. \end{aligned}$$

When all the design parameters are known, the analytical solution of the required resistance R can be obtained through **Eq. 16**. In the next section, the microstrip E-shape resonator is chosen as the basic resonant element to design a dual-band filtering power divider with 90° phase distribution, which verifies the proposed design method.

IMPLEMENTATION AND RESULTS

To validate this design method, a dual-band FPD prototype was designed and fabricated based on the substrate of Rogers RO4003C with a relative dielectric constant $\varepsilon_r = 3.55$, thickness $h = 0.508$ mm, and loss tangent tan $\delta = 0.0027$.

The L/C resonators are all implemented by E-shape resonators as shown in **Figure 3A**, and the external/internal couplings are all controlled through the gap couplings. Based on the aforementioned analytical equation, the required design parameters can be obtained.

For the E-shape resonators, it can be analyzed by means of even/odd-mode analysis, and the odd-mode and even-mode equivalent circuits are shown in **Figures 4B, C**. Based on the even/odd-mode analysis, the resonant frequency of the odd-mode and even-mode can be obtained as [14]:

$$f_{in,odd} = \frac{c}{4(L_1/2)\sqrt{\varepsilon_{eff}}}, \tag{23}$$

$$f_{in,even} = \frac{c}{4(L_1/2 + L_2)\sqrt{\varepsilon_{eff}}}. \tag{24}$$

The odd-mode resonant frequency of two pairs of E-shape resonators is used to construct the dual-band filtering power divider.

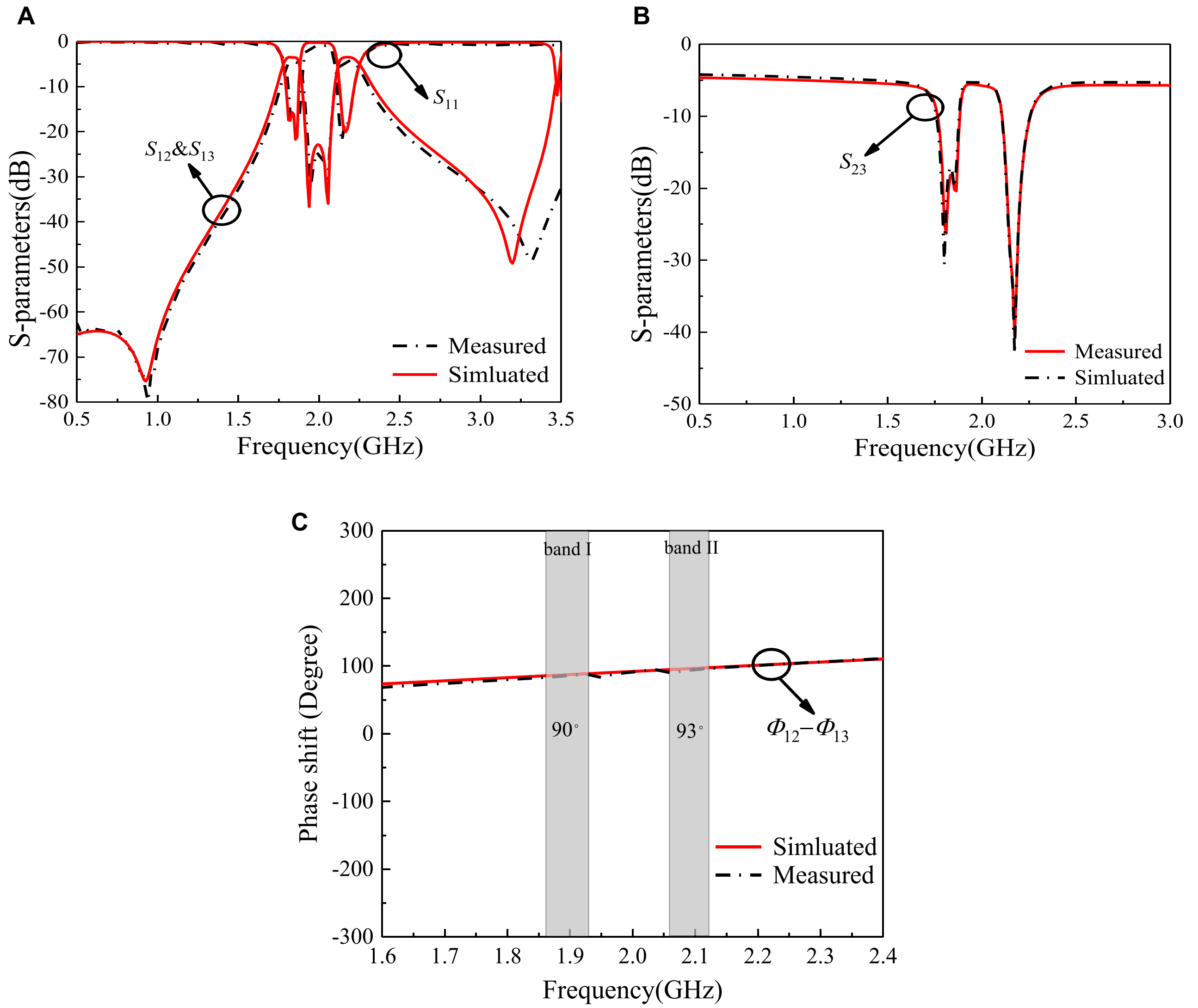

FIGURE 6 | Measured and simulated results of the proposed dual-band FPD. **(A)** Magnitudes of S_{11}, S_{12}, and S_{13}. **(B)** Magnitudes of S_{23}. **(C)** $\angle S_{12}-\angle S_{13}$.

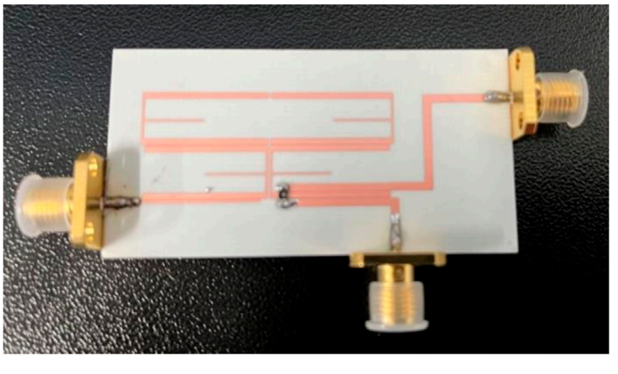

FIGURE 7 | Photograph of the fabricated circuit board.

The whole configuration of the proposed dual-band FPD including corresponding dimensions is shown in **Figure 5**. As observed, there are two pairs of dual-mode resonators between the input port and the output port. The lower pairs of dual-mode resonators are the bandpass resonators, while the upper pairs of dual-mode resonators are the bandstop resonators. The signal is introduced from port #1 and coupled to the arm of the first E-shape resonator. Then, the signal flows through the two pairs of E-shape resonators and is coupled to the two output ports (port #2 and port #3) by the arm of the second bandpass E-shape resonator, which forms a three-coupled line structure. Also, the isolation resistance R is loaded on the front end of the three-coupled line structure to achieve good port–port isolation.

In addition, **Figures 6A, B** exhibit the simulated and measured results of the proposed dual-band FPD. As shown in **Figures 6A, B**, the measured insertion losses are 1.2 and 1.3 dB, respectively, the measured return losses are all higher than 18 dB, and the measured in-band isolation within two output ports is all higher than 16 dB. Moreover, the phase difference between two outputs within the two passbands is about 90° with less than 3° phase imbalance. The photograph of the fabricated circuit board of the dual-band FPD is shown in **Figure 7**. The overall size of the circuit is $0.67\lambda g \times 0.53\lambda g$, where λg is the relative wavelength of the center frequency. In conclusion, the decent results exhibit the feasibility and effectivity of our proposed design method.

CONCLUSION

This study presented a novel synthesis design method of dual-band FPD including arbitrary phase distribution based on the topology of inverter-coupled L/C resonators. A representative dual-band FPD with 90° phase distribution based on E-shape resonators has been designed and fabricated to verify the design method. It is our belief that the proposed method will be very attractive in future multi-functional wireless communication systems.

DATA AVAILABILITY STATEMENT

The original contributions presented in the study are included in the article/Supplementary Material, further inquiries can be directed to the corresponding author.

AUTHOR CONTRIBUTIONS

JS, WL, KP, ZZ provide the idea and write the paper. MS modify the paper.

REFERENCES

1. Wang K-X, Zhang XY, Hu B-J. Gysel Power Divider with Arbitrary Power Ratios and Filtering Responses Using Coupling Structure. *IEEE Trans Microwave Theor Techn* (2014) 62(3):431–40. doi:10.1109/tmtt.2014.2300053
2. Chau W-M, Hsu K-W, Tu W-H. Filter-based Wilkinson Power Divider. *IEEE Microw Wireless Compon Lett* (2014) 24(4):239–41. doi:10.1109/lmwc.2014.2299543
3. Chen C-J, Ho Z-C. Design Equations for a Coupled-Line Type Filtering Power Divider. *IEEE Microw Wireless Compon Lett* (2017) 27(3):257–9. doi:10.1109/lmwc.2017.2661968
4. Bai YC, Xu. KD. High-performance Filtering Power Divider with Multiple Transmission Zeros. *Microw Opt Technol Lett* (2018) 60(11):2673–6. doi:10.1002/mop.31468
5. Xu KD, Bai Y, Ren X, Xue Q. Broadband Filtering Power Dividers Using Simple Three-Line Coupled Structures. *IEEE Trans Compon., Packag Manufact Technol* (2019) 9(6):1103–10. doi:10.1109/tcpmt.2018.2869077
6. Yu W, Xu L, Zhang XY, Chen J-X. Dual-band Dual-Mode Dielectric Resonator Filtering Power Divider with Flexible Output Phase Difference and Power Split Ratio. *IEEE Trans Microwave Theor Techn.* (2022) 70(1):190–9. doi:10.1109/tmtt.2021.3113654
7. Hong W, Jiang ZH, Yu C, Zhou J, Chen P, Yu Z, et al.Multibeam Antenna Technologies for 5G Wireless Communications. *IEEE Trans Antennas Propagat* (2017) 65(12):6231–49. doi:10.1109/tap.2017.2712819
8. Basavarajappa V, Pellon A, Montesinos-Ortego I, Exposito BB, Cabria L, Basterrechea J. Millimeter-wave Multi-Beam Waveguide Lens Antenna. *IEEE Trans Antennas Propagat* (2019) 67(8):5646–51. doi:10.1109/tap.2019.2916388
9. Lyu Y-P, Zhu L, Cheng C-H. A New Design of Filtering Power Dividers with Arbitrary Constant Phase Difference, Impedance Transformation, and Good Isolation. *IEEE Access* (2019) 7:169495–507. doi:10.1109/access.2019.2955104
10. Kim S, Chaudhary G, Jeong Y. Filtering Power Divider with Arbitrary Prescribed Phase Difference. In: 2020 IEEE Asia-Pacific Microwave Conference (APMC) (2020):421–3.
11. Zhu X, Yang T, Chi P, Xu R. Miniaturized Reconfigurable Filtering Power Divider with Arbitrary Output Phase Difference and Improved Isolation. In: 2021 IEEE MTT-S International Microwave Symposium (IMS) (2021):104–7.
12. Hong J-S. *Microstrip Filters for Rf/microwave Applications*. New York, NY, USA: Wiley (2001).
13. Lee B, Nam S, Lee J. Optimization-free Design Equations for Narrowband Equal-Division Filtering Power Divider with Pre-specified Filtering Response and Wideband Isolation. *IEEE Trans Circuits Syst* (2019) 66(7):2496–507. doi:10.1109/tcsi.2019.2898465
14. Tang L, Zhang X, Jiao F, Liu S, Zhang G, Yang J. Design of a Compact Microstrip Triplexer-Power Divider with E-Shaped Resonator. In: 2019 International Conference on Microwave and Millimeter Wave Technology (ICMMT) (2019):1–2.

Conflict of Interest: The authors declare that the research was conducted in the absence of any commercial or financial relationships that could be construed as a potential conflict of interest.